Gigahertz (GHz) hard x-ray imaging using fast scintillators

Zhehui Wang, Elena Guardincerri, D. D. Rathman, M. E. Azzouz, Cris W. Barnes, et al.

Zhehui Wang, Elena Guardincerri, D. D. Rathman, M. E. Azzouz, Cris W. Barnes, R. Berger, E. M. Bond, D. M. Craig, David Holtkamp, J. S. Kapustinsky, Alexei V. Klimenko, K. Kwiatkowski, R. B. Merl, C. L. Morris, J. O. Perry, E. Ramberg, R. K. Reich, A. Ronzhin, K. Warner, R. T. Williams, Ren-Yuan Zhu, "Gigahertz (GHz) hard x-ray imaging using fast scintillators," Proc. SPIE 8852, Hard X-Ray, Gamma-Ray, and Neutron Detector Physics XV, 88521A (26 September 2013); doi: 10.1117/12.2022294

Event: SPIE Optical Engineering + Applications, 2013, San Diego, California, United States

Gigahertz (GHz) hard X-ray imaging using fast scintillators

Zhehui Wang*[a], Elena Guardincerri[a], D. D. Rathman[b], M. E. Azzouz[a], Cris W. Barnes[a], R. Berger[b], E. M. Bond[a], D. M. Craig[b], David Holtkamp[a], J. S. Kapustinsky[a], Alexei V. Klimenko[a], K. Kwiatkowski[a], R. B. Merl[a], C. L. Morris[a], J. O. Perry[a], E. Ramberg[c], R. K. Reich[b], A. Ronzhin[c], K. Warner[b], R. T. Williams[d], Ren-Yuan Zhu[e]

[a] Los Alamos National Laboratory, Los Alamos, NM 87545, U.S.A.; [b] Lincoln Laboratory, Massachusetts Institute of Technology, Cambridge, MA; [c] Fermi National Accelerator Laboratory, Batavia, IL 60510, U.S.A; [d] Department of Physics, Wake Forest University, Winston-Salem, North Carolina 27109, U.S.A.; [e] California Institute of Technology, Pasadena, CA 91125, U.S.A.

ABSTRACT

Gigahertz (GHz) imaging technology will be needed at high-luminosity X-ray and charged particle sources. It is plausible to combine fast scintillators with the latest picosecond detectors and GHz electronics for multi-frame hard X-ray imaging and achieve an inter-frame time of less than 10 ns. The time responses and light yield of LYSO, $LaBr_3$, BaF_2 and ZnO are measured using an MCP-PMT detector. Zinc Oxide (ZnO) is an attractive material for fast hard X-ray imaging based on GEANT4 simulations and previous studies, but the measured light yield from the samples is much lower than expected.

Keywords: GHz X-ray imaging, MCP-PMT detectors, fast scintillators, detection efficiency.

1. INTRODUCTION

Gigahertz (GHz) detector technologies are needed to capture and store the dense spatial and temporal signals produced in inertial confinement fusion, synchrotron and X-ray free-electron laser (XFEL) facilities, and charged particle experiments such as LHC high-luminosity upgrade [1]. Although GHz frame rates are not essential, medical imaging such as PET does require pico-second timing accuracy for high-resolution tomography and therefore overlaps with GHz detector technologies in sensor materials and electronics. High-speed sensing, in the forms of radar and lidar for example, is also becoming essential in autonomous controls of automobiles and other personal devices.

Gigahertz X-ray imaging is about how to record a 2 (space) + 1 (time) dimensional X-ray field with an inter-frame time shorter than 1 ns. Sub-ns detection of X-rays at 5 keV and higher energies typically uses streak cameras or gated framing cameras. Both technologies, however, have known limitations. Streak cameras use up one dimension of the imaging space for time and leave only one dimension available for spatial information. Gated framing cameras, which use multiple pin-holes and delayed sequential fast gating of micro-channel plates (MCPs) for an equivalent GHz rate, suffer from parallax and small spatial dynamic range (defined as the ratio of the size of the field of view to the spatial resolution). The state-of-the art CCD and CMOS cameras, optimized for visible and near infrared light, can record movies at MHz rate along a single line-of-sight [2]. Each image frame is recorded and stored fast enough so that subsequent images can be recorded repetitively.

Imaging at a GHz rate is challenging using any part of the electromagnetic spectrum. In additional to the GHz rate, other challenges in ultrafast hard X-ray imaging include pico-second sensor response, large dynamic range and very high data rate [3]. Hybrid detector configuration, which separates the photon sensors from the electronics, provides flexibility in optimizing the sensor and electronics separately [4][5]. Once electronic data, typically in the form of electric charge stored in one or more capacitors, are generated, the data would require GHz integrated circuits (ICs) for further processing (amplification, analog-to-digital conversion) and storage. Gigahertz ICs are also known as monolithic microwave (0.3- 300 GHz) ICs (MMICs) with mm-wave (30 – 300 GHz) being a subset. Although GHz ICs were first demonstrated using compound semiconductors (GaAs) as early as 1960s [6], their usage has largely been hampered by

* Email: zwang@lanl.gov; phone: (505) 665 5353

Hard X-Ray, Gamma-Ray, and Neutron Detector Physics XV, edited by Michael Fiederle, Arnold Burger, Larry Franks, Ralph B. James, Proc. of SPIE Vol. 8852, 88521A · © 2013 SPIE
CCC code: 0277-786X/13/$18 · doi: 10.1117/12.2022294

the high cost of compound semiconductor fabrication and processing. Processing in CMOS the least expensive IC technology. Silicon transistors and SiGe (IBM) transistors can now operate above 100 GHz and even at one Teraherz (THz) [7][8]. The imaging rate is lower than the transistor or clock rate since it takes multiple transistor or clock periods to process and record a signal. Millimeter-wave CMOS circuits have made steady progress in speed and overall performance, tracking the progress in the shrinking feature-sizes in micro-fabrication. 130-nm bulk-CMOS technology is capable of power gain at 60 GHz [9][10][11].

There are two generic approaches to X-ray sensing, as summarized in Fig. 1. Both methods collect as signals the secondary particles produced by X-ray-matter interactions. One is to collect electron-hole pairs, as in semiconductors and photoconductors. The other is to collect photons, as in scintillators and some semiconductors. Both types of materials can come in amorphous powder forms or crystalline forms. The electron-hole approach has delivered excellent spatial resolution, which may ultimately be limited by the stopping range of photoelectrons. In silicon at 40 keV, for example, the continuous slowing-down range of electrons is 3.8 x 10^{-3} g/cm^2 or less than 20 um in distance. Compton scattering becomes significant for 40 keV and higher energy X-rays, generating background that may not be negligible in low-Z materials. Furthermore, electron and hole drift velocities limit the recovery time of silicon and other semiconductor detectors. Even in a high-mobility semiconductor like GaAs, which has an electron drift speed close to 2 x 10^7 cm/s and is about a few times faster than that of silicon [12], 1 ns would correspond to a sensor thickness of 200 um, which is still not thick enough for an efficient detection of 40 keV and higher energy X-rays. Although the speed of signal propagation is not an issue for scintillators, visible photons generated by X-ray are emitted isotropically into 4π solid angles, resulting in a poor spatial resolution. In short, direct use of crystalline or amorphous forms of either semiconductor or scintillator may not be able to achieve GHz hard X-ray imaging with high efficiency and adequate spatial resolution simultaneously. Both material types will require some forms of microscopic structures, or '3D structures', to be effective.

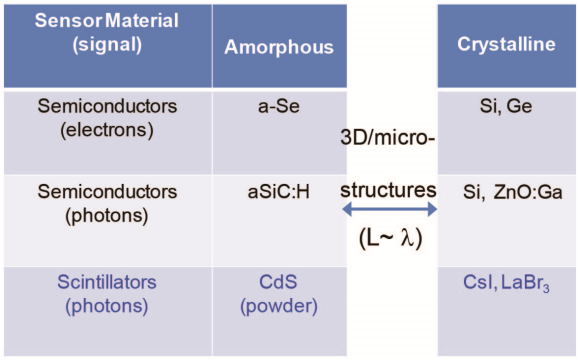

Figure 1: Two generic types of X-ray sensors are semiconductors and scintillators. Each type can be divided into amorphous powder and crystalline forms. Efficient GHz X-ray detectors may require microscopically structured, or "3D structured" materials in either approach.

Here we focus on using fast scintillators and in particular inorganic scintillators as sensors. Organic scintillators with a fast decay time on the order of 1 ns are commercially available, but Compton scattering could become a significant issue for high-spatial-resolution (comparable to the electron stopping range) imaging. Below, we first present some results from a GEANT4 simulation and analysis for 42 keV X-rays and make comparisons with silicon. Next we present some experimental data on various detectors and scintillators, and evaluate their usage as building blocks for pixilated array detectors. We then discuss conceptual designs for fast hard X-ray imagers operated at around one GHz rate.

2. COMPARISON OF SENSOR MATERIALS

Spatial resolution, efficiency and frame rate dictate the design of pixelated GHz X-ray sensors and the selection of sensor material and geometric structures. Data handling (A-to-D conversion, transmission and storage) can be separated from the sensor development in hybrid detector architectures. X-ray absorption length and detection efficiency can be calculated accurately based on the tabulated cross sections of X-ray photons in materials with known molecular compositions. Secondary particles, including photoelectrons, Compton electrons, Auger electrons, fluorescent X-rays, lower energy electrons and visible light require much more detailed consideration of particle tracks, specific material

properties and can only be effectively treated using computers. When the number of primary particles is small and the resulting number of secondary particles is too small to fill up the allowable phase space, the detectable signals can also fluctuate significantly from the mean values expected of a large ensemble of identical incident X-rays. Material properties and geometrical structures, such as impurities, defects, spatial variations of refractive index, grain size distribution, vary from sample to sample, and their effects on X-ray detection can even be difficult to predict computationally and thus would require experimental measurements. Here the spatial resolutions of X-ray sensors have been studied using GEANT4 simulations. Material properties are assumed to be uniform and isotropic for simplicity. The studies allow us to down-select potentially interesting materials for X-ray sensing and experiments.

2.1 Silicon and high-Z semiconductors

Silicon has been the sensor material of choice in pixelated X-ray detectors for a combination of facts. Low-defect large-area wafers are readily available. Material properties are tunable through doping. The CMOS process is mature and relatively inexpensive. Both monolithic and hybrid schemes have been demonstrated for sensor and electronics (ASIC) integration. As a result, silicon X-ray imagers have achieved excellent spatial resolution at near 10 MHz frame rate and X-ray energies up to 15 keV.

Attempts to develop GHz imagers for 40 keV and harder X-rays using silicon face several fundamental physical constraints. Silicon has low X-ray stopping power and a Compton scattering fraction above 21%. Thick silicon wafers exceeding 1 cm thick will be required for efficient X-ray detection at 40 keV. On the other hand, the carrier mobility makes silicon sensors too slow if the electrons have to drift for a 1-cm distance. Innovative schemes for electron collection, such as edge-on detection and using a matrix of electrodes with micrometer spacing, can potentially reduce the electron drift distances to about 10 um, and thus reduce the electron collection time to about 1 ns. These innovative schemes remain to be demonstrated. The large Compton scattering fraction reduces the spatial resolution of silicon devices significantly from the photoelectron range, see Figure 5 below.

High-Z semiconductors, in particular Ge, GaAs, CdTe, are attractive to GHz hard X-ray imaging because only 1/10 or less of the silicon thickness would be needed for high detection efficiency (above 90%). Higher carrier mobilities in Ge and GaAs can lead to higher frame rates. However, besides high fabrication cost, innovations in material, detector design and fabrication, packaging would be needed to turn these advantages into practical devices. Germanium detectors need to operate at the liquid nitrogen temperature. The defects in GaAs need to be controlled. The electron mobility in CdTe at room temperature is 1000 cm^2/Vs, less than that of Si (1400 cm^2/Vs). Radiation damage is an additional concern when using these high-Z semiconductor imagers in a high-luminosity environment, in particular because these imagers are expected to be used repetitively.

2.2 Fast Scintillators

X-rays can be converted into visible and UV photons using scintillators through photoelectric absorption or Compton scattering. Holes and free electrons are created in both processes [13]. A hole is the atom that loses an inner shell (most likely K-shell, then L-shell and so forth) electron. More methods are available to detect visible and near infrared (1300 to 1550 nm in particular) photons efficiently and faster than possible in other parts of the electromagnetic spectrum.

The list of fast scintillators is rapidly growing due to interests from medical imaging, homeland security, and other fields. Essentially all scintillators are compound insulators. Most scintillators can readily achieve 90% and above attenuation within a thickness of 1 mm, Figure 2. Most attenuation is attributed to photoelectric absorption, Figure 3. Although no material is an obvious choice for a GHz imager, quite a few of them can be used to achieve frame rates above 100 MHz, as discussed below.

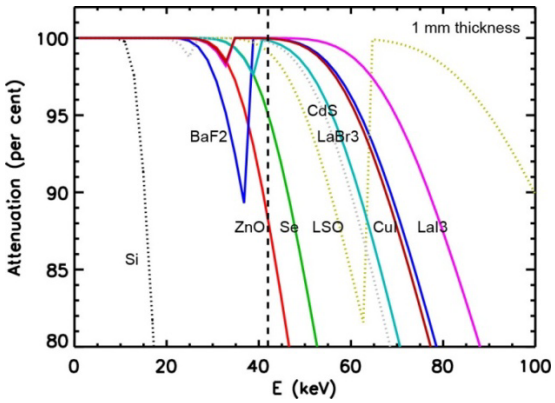

Figure 2: Attenuation of X-ray as a function of X-ray energy in various scintillators with 1 mm thickness, in comparison with Si and Se. One mm or thinner is sufficient for 42 keV X-rays for most of the scintillators.

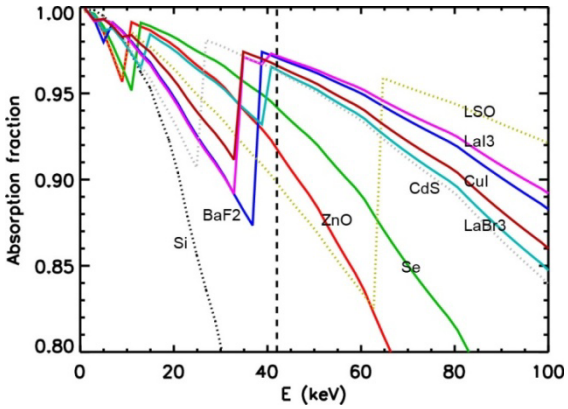

Figure 3: Fraction of photoelectric absorption in various scintillators, in comparison with silicon and selenium.

2.3 Energy deposition and spatial resolution

We developed a custom application using GEANT4 to evaluate the energy deposition and spatial resolution of the scintillators shown in Figure 2 and Figure 3 for 42 keV X-rays. Individual 42 keV photons reach a flat surface of a material at normal incidence. The physics list (that is, the collection of physics models) is 'Penelope', which includes the low-energy models for $e^{\pm}$ and γ-rays from the Monte Carlo code PENELOPE [14]. For 42 keV X-rays, only photo-absorption, coherent (Rayleigh) and incoherent (Compton) scattering are relevant. Positron (e^{+}) physics can be ignored. Coherent interactions of optical photons with the material, which could degrade the spatial resolution further, were not considered.

The calculated energy depositions are shown in Fig. 4. The results are based on 10000 X-ray photons per material. Since the size of the sample is much greater than the ranges of incident X-rays and secondary particles, the derived energy depositions can be called the maximum allowable energy deposition for each sample. The reason that the maximum allowable energy deposition is less than the initial 42-keV incident photons is due to Compton back scattering and coherent back-scattering of the incident X-rays, which cause a fraction of the initial energy to leak out of the sample. The energy deposited ranges from 0.84 (BaF_2) to more than 0.99 (LSO) of the initial photon energy. Poly (CH_2), which approximates an organic scintillator, is also included here for comparison.

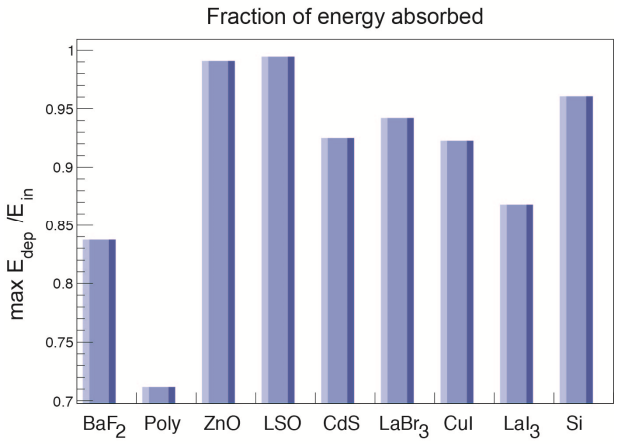

Figure 4: Fraction of the allowable 42-keV photon energy deposition in various scintillators and in comparison with Si.

The corresponding spatial resolution in terms of energy deposition is shown in Figure 5. The longitudinal (thickness) and lateral (width) spatial resolution with respect to the incoming photon direction is defined for 90% of the maximum allowable X-ray energy deposited (Figure 4). With a sensor thickness of more than 1.8 cm and a lateral width near 0.6 cm, pixel resolution using Si will be around 6 mm, too coarse for many high-resolution imaging applications using a coherent X-ray source. Two materials that stand out in terms of fine pixel resolution are ZnO and LSO.

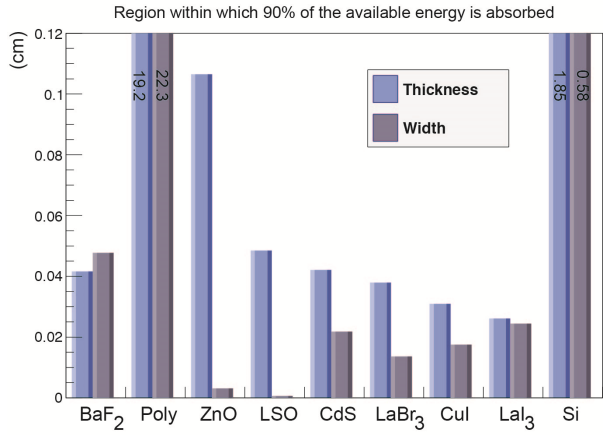

Figure 5: The depth (thickness) and width of the region within which 90% of the total energy deposition (Figure 4) reside.

The variations of the energy-deposition width for different materials in Figure 5 can be understood by the combination of the edge structure of X-ray absorption, Z-dependences of the Auger electron/fluorescent X-ray yield and of the Compton scattering. The atomic cross section for Compton scattering is proportional to Z, or the number of electrons in the atom. The annihilation of the holes created within an atom (most likely in either the K-shell or the L-shell, depending on Z) after photoelectric emission can result in Auger electron emission or fluorescent X-ray emission. The fraction of K-shell Auger electron emission is higher than 0.5 for Z less than ~ 32 (Ge). Since the typical CSDA range of photoelectrons generated by interactions of 42-keV photons is a few tens of μm (CSDA range of 40 keV electron is 16 μm in Silicon and 9.4 μm in Germanium), energetic electrons, due to either photoelectric or Auger emission, do not cause any significant spread of the initial X-ray energy across the material. It is either the ranges of fluorescent X-rays or Compton X-rays that determine the overall energy deposition range in matter. The K-edge for Zn is at 9.776 keV, and all the X-rays from KL and KM transitions have energies between 8.4 keV and 9.7 keV: such photons are mostly contained within few tens of μm around their point of origin. As a result, the lateral spread in ZnO is among the smallest. In BaF_2, the K-edge energy is at 37.4 keV and all the X-rays from KL and KM transitions have energies between 31.4 and 37.4 keV, enough for them to travel hundreds of μm from their point of origin before absorption. For even higher Z materials, the K-edge is too high for 42-keV absorption. In LSO, for example, the K-edge for Lu is 63.3 keV, then the absorption is due to L-shell electron, where again the energy of the incident 42-keV x-rays is mostly confined close to the beam

direction. It is clear that a thick scintillator is beneficial in order to maximize the detection efficiency for X-ray photons, but for some materials (e.g. BaF_2) this comes at the expense of a poor spatial resolution.

3. CHARACTERIZATION OF SCINTILLATORS AND DETECTORS

Characterization of the combined scintillator and detector time response, light yield and efficiency can be useful for scintillator selection and GHz imager design. We used an alpha-tagged X-ray source (^{241}Am) to characterize the scintillators and detectors. The three characteristic nuclear X-ray lines are 13.9 keV (37%), 26.3 keV (2.3%) and 59.5 (35.9%). For a 1 cm^2 sensor area and a time window of detection of 1 us, the alpha particle signal can reduce the absolute number of false signal rate due to background cosmic rays to 1.7 x 10^{-8} Hz. For a low overall detection efficiency of 10^{-2} Hz, the relative false rate is still only 1.7 x 10^{-6} Hz. The experimental setup is illustrated in Figure 6.

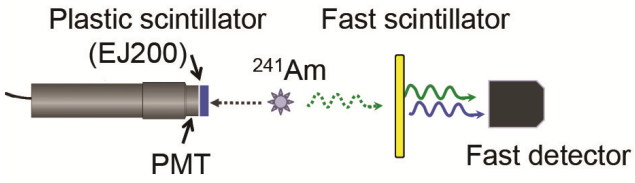

Figure 6: An ^{241}Am source is used to characterize the scintillator and detector response time, light yield.

We compare the time responses of some fast detectors, Figure 7. Each of the measurements corresponds to either single cosmic rays (Photek VMCP-PMT 210, Photek MCP-PMT 240) or single photon (STM SiPM, MPD APD). The VMCP-PMT does not have a glass window or a photocathode. The longer decay time for the MCP-PMT 240 is likely due to the combined light and photoelectron spread before reaching the MCPs. In Figure 8, we show that it may be possible to take multiple pulses as fast as 5 ns apart, corresponding to a frame rate of 200 MHz. The detector here is the MCP-PMT 240. Proton beams were used for the measurement. The estimated number of protons was 10^4 to 10^5 elementary charges per pulse.

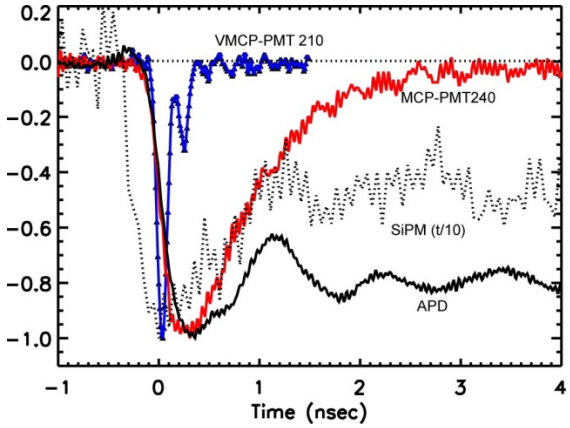

Figure 7: Sub-ns rise-time and longer decay time of various fast detectors, except for SiPM (which has a rise-time of a few ns[†]).

[†] It should be pointed out that SiPM's can operate with sub-ns rise time, much faster than the measurement shown here.

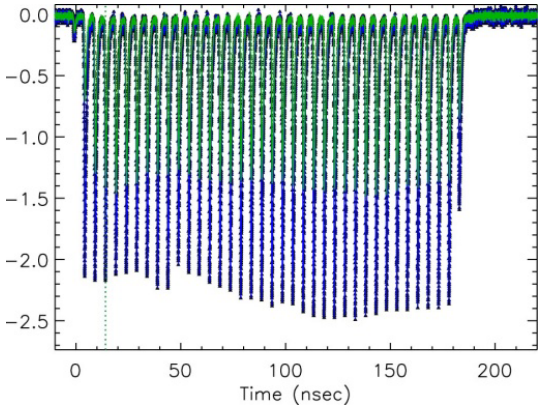

Figure 8: Proton pulse train response of the MCP-PMT detector, the inter-pulse time is 4.96 ns.

We measured the response time and relative light yield from a few scintillators using an ^{241}Am source. The results are shown in Figure 9. When there is plenty of light, as in $LaBr_3$ and LYSO, the signal can be fitted using the following model

$$I(t) = I_0(e^{-t/\tau_0} - e^{-t/\tau_r}), \tag{1}$$

with τ_0 being the decay time and τ_r the rise time. The BaF_2 crystal, about 1 cm thick, emits a short pulse of photons within the expected fast decay time of less than 1 ns, followed by additional emission of other photons that lasts much longer, consistent with the expected slow decay component of BaF_2. However, given the small number of photons and the fast response of the MCP-PMT detector, the longer decay time component shows up as randomly emitted single photon-level signals that last hundreds of ns, longer than the data acquisition window of the DRS4 used here. Zinc Oxide (ZnO), (Goodfellow ZN522010, single crystal, 1 mm thick nominal) emits so little light that the signals show up as randomly emitted single photon-level pulses that also spread out over tens of nanoseconds.

.

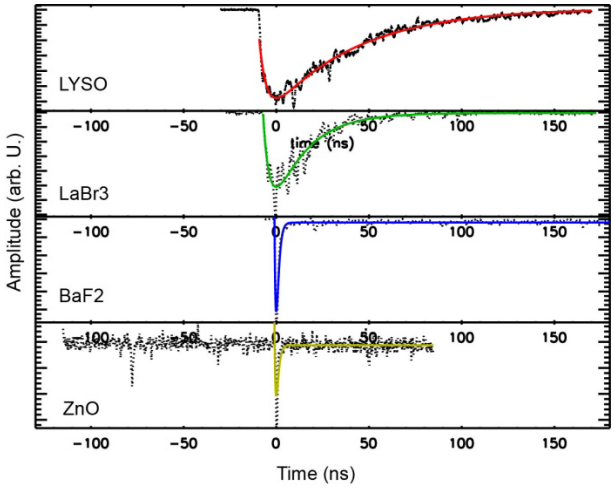

Figure 9: Time response and light output from several scintillators. A Photek MCP-PMT 240 detector was used.

4. CONCEPTUAL DESIGN FOR GHZ HARD X-RAY IMAGER

One possible approach to GHz hard X-ray imaging is to use the hybrid configuration that combines a pixelated fast scintillator and a picosecond detector array with a fast pixelated ASIC chip. A GHz ASIC chip is desirable but not necessary depending on the scintillator and detector arrangement. Compared with semiconductors, scintillator sensors

have lower spatial resolution in imaging applications because the visible photons are normally emitted into 4π solid angle and the mean free path of the photons are much greater than the scintillator thickness of a few mm. One way to improve the spatial resolution in scintillators is to pixelate the scintillator so that visible photons and other secondary particles produced in each pixel is contained within a pixel [15][16]. According to Figure 5, however, the physical size of a pixel is not the only determining factor for resolution. Fluorescent and Compton X-rays are the most penetrating among the secondaries. There are several approaches to implementing the idea of pixelated scintillators. In some scintillators like CsI(Tl), columnar structure can form. Another approach is to 'fill' micro-capillary arrays with micrometer or smaller particles or use vapor deposition methods to fill up the voids. A third approach is laser micro-cutting of a bulk scintillator. A fourth approach is to fuse microfibers together. Many microstructures are available commercially. In each approach, the efficiency and resolution of detection depends on the material, texture, size and length of the pixels and will need experimental characterization. Fiber optics faceplates could be used to couple the pixilated scintillator array to the detector array.

4.1 Fast scintillator options

Light yield as a function of wavelength and light 1/e-decay time are important factors in choosing scintillators for GHz imaging. Thallium-doped sodium iodide, NaI(Tl), with a light yield of 38 photons/keV, or 26-eV energy consumption per photon, is typically used as the reference material for comparison. Thallium-doped cesium iodide, CsI(Tl), is widely used in medical X-ray imaging because of its high light yield of 54-65 photons/keV. The 1/e-decay time of CsI(Tl) is about 1000 ns. Undoped CsI, in contrast, has only a light yield of 4.7% of NaI(Tl), 1.8 photons/keV, of which, 23% comes from the fast decay component (6 ns), or 0.4 photons/keV. The remainder of the photons comes from the slow component (30 ns), or 1.4 photons/keV. The light yield of BaF_2 is 1.5-1.8 photons/ keV for the fast component, and 8-11 photons/ keV for the slow component [17]. The light yield of $Lu_{2-x}Ce_x(SiO_4)O$ (LSO) is about 50 to 75% of that of NaI(Tl) [18]. The light yield of LYSO:Ce is about 85% of that of NaI(Tl), or 32 photons/keV. The light yield of $LaBr_3$ is about 1.53 times that of NaI(Tl). These results are consistent with the measurement shown in Figure 9, except for ZnO:Ga, from which a much higher light yield is expected according to powder measurements [19][20]. Besides material structure and doping concentration, another possible explanation is self-absorption, which limits light escape from only within a very shallow distance from the surface [21]. Some additional materials of potential interest are summarized in Table 1.

Table 1. A possible selection of scintillators for fast imaging [22].

Scintillator	Peak Wavelength (nm)	Transition time (ns)	Light yield (ph/keV)
CsI [23]	310-315	6/30	7
BaF_2 [17] [24]	220/300	0.8/600	1.5/11
Lu_2SiO_5:Ce (LSO)	420	12/42	19-28
(Lu,Y)2SiO5:Ce (LYSO) [25]	402/420	40	27
$LaBr_3$:Ce [26]	356	20	58
LaI_3:Ce [27]	452, 502	1-2 ?	16 (T = 100k)
CsF [28]	390	2.9	2
HfO_2	480	9.5	31
RbF	203/234	1.3	1.7
ZnO:Ga [29]	385 -389	0.36/0.82	9.7-15 [T=12K]
CdS:In (powder)	519	<1	1 [T=12k]

CuI (powder)	420-430	<1	2 [T=12k]
HgI_2 (powder)		<1	12 [T=12k]
PbI_2 (powder)		<1	3 [T=12k]

4.2 Picosecond photodetectors

The conventional photocathode approach to convert UV and visible light to electrons suffers from low quantum efficiency (QE), that is, QE below ~ 30%. In contrast, back-illuminated CCD (Si) can achieve QE above 90% for certain visible photons. Many factors, such as reflection, various electron loss mechanisms within the cathode, surface morphology, and aging, can lower the QE. In addition to cathode material research that now extends to compound semiconductors, nanostructured photocathodes, which contains regular structures much smaller than the wavelengths of visible light, may also be promising in improving the QE in the near future.

Selecting appropriate photocathodes that match the scintillator emission spectrum, together with a multi-anode MCP structure for electron multiplication and fast electronics for analog data storage and A-to-D conversion, is one approach to GHz hard X-ray imaging. Micro-channel plate-based detectors lend themselves naturally to pixilated imaging, and have demonstrated photon-counting time resolutions superior to solid-state devices such as the APD's or SiPM's [30][31]. The spatial resolution, dead-time (in high-gain mode), optical and electrical cross talk, and high cost associated with scaling up the detectors (from 10 x 10 arrays to 1k x 1k arrays) are potential obstacles.

A second class of picosecond photodetectors is solid state devices, in particular photodiodes (APD's) and their higher-gain counterparts, Geiger-mode avalanche photodiodes [32]. Besides silicon, which detects 400 - 500 nm photons with efficiencies close to 90%, other semiconductor PD's and APD's are also available to match other wavelengths in the UV, visible, and infrared segment of the electromagnetic spectrum. Besides the advantage of doing away with a vacuum envelope, solid-state devices are easier to integrate with data collection and processing ASICs and ROICs at low cost. Spatial resolution can approach those of CCD's, or a few um. By using a scintillator sensor in front, the radiation damage problem within high-speed electronics is also mitigated. Time jitter, long dead-time (10s of ns), electrical cross talk at high gain, and dark counts are potential issues that are being addressed.

A short summary of the different picosecond photodetectors is given in Table 2. It is worthwhile to note that these detectors are all sensitive to single photons. The quantum efficiency (QE) or photo detection efficiency (PDE) is for visible photons. For hard X-rays, a scintillator can produce the number of visible photons many times that of incident X-rays. We also include novel superconducting single-photon detectors (SSPD) that use nanowires. In addition to the need for a cryogenic environment and challenges in scaling up to large 2D arrays (megapixels), their QE's are quite low at the moment.

Table 2. Comparison of picosecond detectors.

Detector type	Detection rate (MHz)	QE/PDE (%)	Time jitter (ps)	Dark counts (Hz)
Multi-anode MCP-PMT	> 6	10-30	10	low
SiPM/MPPC	10	20-80	100	10^4 -10^6/mm^2
SSPD	>1000	<1	20	low

4.3 Gigahertz electronics

The Massachusetts Institute of Technology Lincoln Laboratory (MIT-LL) is working with Ziptronix, Inc. to hybridize the CMOS high speed ROICs with Geiger-mode APD's and thinned back-illuminated Si photodiode detector arrays. When used with fast scintillators that can convert hard X-ray photons to UV-VIS photons in the 250-450 nm range, it is feasible to achieve a GHz imaging rate. The Si photodiodes are thinned from 5-20 μm thick depending on the desired trade-off between quantum efficiency and transit-time-limited speed. At a saturated carrier (electron) velocity of 10^7

cm/sec in silicon, the detector provides a transient response on the order of 10 ps per μm thickness. The detector array has many special features including 2 layers of grid metal and tungsten-filled thru holes (to the diode front surface) to ensure that the return current path for holes (electrons are the collected and stored charge carrier) has extremely low resistance so as not to limit the detector transient response. Even with these features array diode breakdown voltages have been measured to be in excess of 25V, which is more than enough to ensure saturated carrier velocity collection for the detector array thickness.

The CMOS effort is built upon an MIT-LL and Lawrence Livermore National Laboratory (LLNL) collaboration that incorporated an H-tree distribution structure [33]. The H-tree architecture provides equal electrical path lengths to each pixel combined with a fast falling edge (< 50ps) shutter (trigger) signal that is maintained throughout the H-tree array by a series of unbalanced n- and p-MOSFET buffer/repeaters [34]. Validation of the design concepts were demonstrated on a 64 × 64 CMOS test imager where skew test circuits were used to determine skew between the nearest neighbor pixels to be < 3ps. The 64 × 64 ROIC also contained within most of the pixels a very fast response (< 20 ps for λ ~ 400 nm) photodiode for optical testing. By illumination of the diode array using a 200 fs pulse width, frequency doubled (λ~ 400 nm) Ti:Sapphire laser the temporal profile of a gate exposure pulse as short as 100ps was demonstrated for the shortest delay setting. The 64 × 64 ROIC was used to validate the design of 512 x 512 ROIC with four 256 × 256 quadrants. The four quadrants were designed to enable either independent shutter control of each quadrant from four independent falling edge-signals or common shutter control from a single signal via the H-tree network. Operation of the imager with four independent signals enables the capture of four sequential images even though each pixel contains a single-storage site. This quad trigger mode of operation was tested optically by LLNL using short-pulsed illumination from a Ti:Sapphire laser (λ~400nm) and the same fast photodiode design that was built-in to the pixel and used in the 64 × 64 test ROIC. The image capture data demonstrated independent sequential triggering of the four quadrants with 250-ps exposures temporally spaced approximately 100 ps between each quadrant exposure. These results were reported at the 2012 SPIE conference on Target Diagnostics Physics and Engineering for Inertial Confinement Fusion [35].

The next phase is to design a 4-sample 64 × 64 test ROIC capable of sub-ns exposures along a single line-of-sight. The 4-sample design approach still relies on the use of an H-tree and fast falling edge shutter signal to deliver fast and simultaneous multiple exposures across the ROIC. There was also an additional desire to be able to vary and select both the exposure interval for the four samples as well as the inter-frame time. To derive four exposure samples (pulses) with selectable widths and inter-frame times from the single falling-edge shutter signal requires a significant amount of logic circuit elements. For the local neighborhood distribution, it is desirable to distribute pulses, rather than edges, around the pixel community. Many fewer interconnects are required and less logic needs to be replicated in every pixel. The exposure control logic (to enable 8 sequential selectable exposures plus 4 selectable inter-frame intervals) is placed into the middle of each 8 × 8 pixel neighborhood. A pulse buffer has been designed which is capable of being able to fan out 125-ps pulses across an 8 × 8 pixel neighborhood (see Figure 10 and Figure 11 below). During the time period when the exposure pulses are not activating the capture/storage of collected charge for a given sample, provision must be made to sink photocurrent before, in between and after the exposure times are generated at each pixel. The signal waveform for removing photocurrent must be complementary to the exposure pulse sequence assuming p-MOSFETs are used for both collecting and sinking photocurrent. This sink current is formed in each pixel and derived from the exposure pulse sequence.

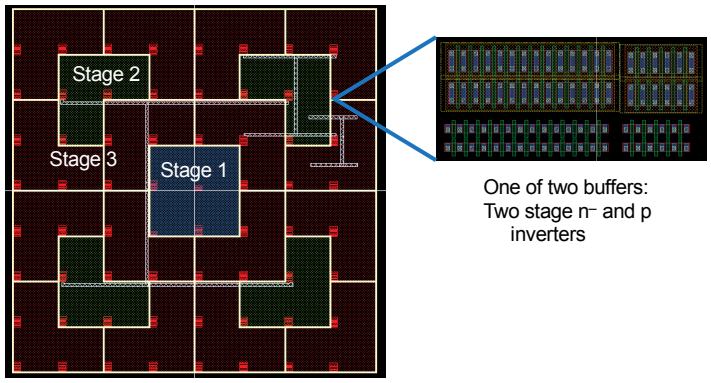

Figure 10: Buffer tree layout for an 8×8 pixel neighborhood (60-μm pixel). There are five signals (four exposure samples and one signal dump), each requiring a three-stage buffer tree (1+4+16=21 buffers per tree) leading to a total of 105 buffers in 64 pixels.

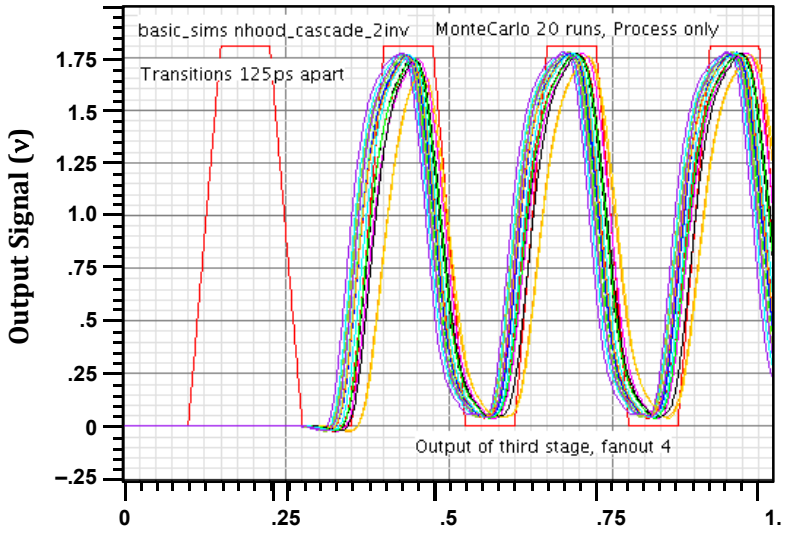

Figure 11: Twenty-run Monte Carlo simulation results for neighborhood buffer tree including wiring parasitics for transition pulses 125ps apart. The multiple traces reflect the differences due to expected process variations with the IBM 7RF process.

The 4-sample 64 × 64 CMOS test ROIC design (~ 70% completed) is intended for fabrication in the MOSIS 180nm IBM7RF process. Characterization of the test ROIC to validate the 4-sample design concepts would be expected to commence a few months after fabrication. It can be mentioned that MOSIS-IBM 8RF (130 nm CMOS) technology is also an option for faster electronics [36].

5. SUMMARY AND CONCLUSION

Gigahertz (GHz) imaging technology will be needed at high-luminosity coherent X-ray and charged particle sources. A few GHz is close to the existing speed limit of CMOS electronics. Photonics are intrinsically faster than electronics. However, optical signals need to be converted to electrical or magnetic signals for information storage. Signal processing is also dominated by electronic methods. It is plausible to combine fast scintillators with the latest picosecond detectors and GHz electronics for fast multi-frame hard X-ray imaging and achieve an inter-frame time of less than 10 ns. The time response and light yield of LYSO, $LaBr_3$, BaF_2 and two different ZnO samples were measured using an MCP-PMT detector. Zinc Oxide (ZnO) is an attractive material for fast hard X-ray imaging according to GEANT4 simulations and previous studies, but the light yield from the samples is much lower than expected.

ACKNOWLEDGEMENT

We would like to thank Drs./Mr. Bernhard Adams (Argonne National Lab), Jeff Bacon, Nick Bertone (PicoQuant), Karen Byrum (Argonne National Lab), Sergio Cova (Politecnico di Milano, Italy) and his team, Marcel Demarteau (Argonne National Lab), Stephen Derenzo (Lawrence Berkeley Lab), Chien-min Gao (Univ. Chicago), Heinz Graafsma (DESY/Germany), Sol Gruner (Cornell Univ./CHESS), Zhong He (Univ. Michigan), Warren Hsing (Lawrence Livermore National Lab), Chris Kenney (Stanford Univ./LCLS), Nick King, Stuart Kleinfelder (UC Irvine), Anil Mane (Argonne National Lab), Haruo Miyadera, Ken McClellan, Pat McGaughey, James Moody (Lawrence Livermore National Lab), Howard Nicholson (Argonne National Lab), John Oertel, Serge Oktyabrsky (SUNY Albany), Adam Para (Fermilab), David Pennicard (DESY/Germany), James Proudfoot (Argonne National Lab), Alan Teruya (Lawrence Livermore National Lab), Anton Tremsin (UC Berkeley), Mike Ulibarri, Scott Watson, Xianghui Xiao (Argonne National lab), Steve Vernon (Lawrence Livermore National Lab), Liyuan Zhang (Caltech) for discussions and/or help. The DRS4 board was developed by Stefan Ritt (stefan.ritt@psi.ch) of Paul Scherrer Institute. The proton measurements were performed at the Los Alamos proton radiography (pRad) facility with the help from the pRad team. LLNL funded the MIT-LL CMOS prototype imager work.

REFERENCES

[1] P. Lecoq, Can transient phenomena help improving time resolution in scintillators, SCINT 2013, Shanghai, 14-19 April, (2013).

[2] http://www.visionresearch.com/; http://www.**princetoninstruments**.com; http://www.teledyne-si.com

[3] Z. Wang, C. L. Morris, J. S. Kapustinsky, K. Kwiatkowski and S.-N. Luo, Towards hard X-ray imaging at GHz frame rate, Review of Scientific Instrument 83: 10E510 (2012).

[4] H. Graafsma, in [Semiconductor Radiation Detection Systems], K. Iniewski (ed.), CRC Press/Taylor & Francis, Boca Raton, FL (2010), p. 217.

[5] S. M. Gruner, "X-ray imaging detectors, " Phys. Today 65(12), 29-34 (2012).

[6] I.D. Robertson and S. Lucyszyn (eds.), [RFIC and MMIC Design and Technology], Inst. Eng. Technol., London, U.K. (2001).

[7] A. M. Niknejad and H. Hashemi (eds.) [mm-Wave Silicon Technology, 60 GHz and Beyond], Springer, Berlin (2008)

[8] T. S. Rappaport, J. N. Murdock, and F. Gutierrez, "State of the art in 60-Ghz Integrated Circuits and Systems for Wireless Communications," Proc. IEEE 99(8), 1390-1436 (2011).

[9] C. H. Doan, S. Emami, A. M. Niknejad, and R. W. Brodersen, "Design of CMOS for 60GHz applications," in IEEE Int. Solid-State Circuits Conf. Dig. Tech. Papers, Feb. 2004, pp. 440-441.

[10] A. K. Ezzeddine, "Advances in Microwave & Millimeter-wave Integrated Circuits," National Radio Science Conference, 1-8 (Mar., 2007).

[11] A. . Hajimiri, "mm-Wave Silicon ICs: Challenges and Opportunities, " IEEE Custom Integrated Circuits Conference, Sept., 741- 747 (2007).

[12] http://www.ioffe.ru.

[13] P. A. Rodnyi [Physical Processes in Inorganic Scintillators], CRC Press, Boca Raton (1997).

[14] F. Salvat, J.M. Fernández-Varea and J. Sempau, PENELOPE-2011: A Code System for Monte Carlo Simulation of Electron and Photon Transport OECD NEA Data Bank/NSC DOC(2011)/5 (OECD Nuclear Energy Agency, Issy-les-Moulineaux, 2011) http://www.oecd-nea.org/dbprog/courses/penelope-2011.pdf.

[15] J. A. Rowlands, J. Yorkston: Handbook of Medical Imaging, Vol. 1, ed. by J. Beutel, H. L. Kundel, R. L. Van Metter (SPIE, Washington 2000) Chap. 4. and references therein for the various flat-panel X-ray image sensors

[16] M. Simon, K.-J. Engel, B. Menser, X. Badel and J. Linnros, "Challenges of pixilated scintillators in medical X-ray imaging," Nucl. Instrum. Meth. A 591(1), 291-295 (2008).

[17] B. P. Sobolev, E. A. Krivandina, S. E. Derenzo, W. W. Moses and A. C. West, in Proc. MRS Symposium P-Scintillator and Phosphor Materials, Cambridge, 1994, edited by P. Lecoq, W. M. Yen, R. C. Ruchti, M. J. Weber, C. Woody and R.-Y. Zhu. (Cambridge University, Cambridge, 1994), P. 277

[18] C. L. Melcher, J. S. Schweitzer, C. A. Peterson, R. A. Manente and H. Suzuki, [Crystal growth and scintillation properties of the rare earth orthosilicates. Inorganic Scintillators and Their Applications], Delft Unviersity Press (SCINT95), ISBN 90-407-1215-8, :309-315, 1996.

[19] S. E. Derenzo, M. J. Weber, W. W. Moses and C. Dujardin. Measurements of the intrinsic rise times of common inorganic scintillators. IEEE Transactions on Nuclear Science, 47:860-864, 2000.

[20] E. D. Bourret-Courchesne, S. E. Derenzo, and M. J. Weber. Development of ZnO:Ga as an ultra-fast scintillator. Nuclear Instruments & Methods in Physics Research Section a-Accelerators Spectrometers Detectors and Associated Equipment, 601:358-363, 2009.

[21] W. Lehmann. Optical Absorption Edges of ZnO and CdS. Journal of The Electrochemical Society, 112:1150-1151, 1965.

[22] If the source of data is not explicitly given, it is based on Stephen Derenzo, Martin Boswell, Marvin Weber, and Kathleen Brennan, "Scintillation properties," http://scintillator.lbl.gov/.

[23] Zong-ying Wei et al, Nucl. Instrum. Meth. Phys. Res. A, 326 (1993) 508-512.

[24] D.-A. Ma and R.-Y. Zhu, "Light attenuation length of barium fluoride crystals," Nucl. Instrum Meth. A 333, 422-424 (1992).

[25] J. T. M. d. Haas and P. Dorenbos. Advances in Yield Calibration of Scintillators. IEEE Trans Nucl Sci, 55:1086-1092, 2008.

[26] http://hep.caltech.edu/~zhu/.

[27] A. Bessiere, P. Dorenbos, C. W. E. van Eijk, K. W. Kramer, H. U. Gudel, C. D. Donega and A. Meijerink. Luminescence and scintillation properties of the small band gap compound LaI3 : Ce3+. Nuclear Instruments & Methods in Physics Research Section A-Accelerators Spectrometers Detectors and Associated Equipment, 537:22-26, 2005.

[28] C. van Eijk, J. Andriessen, P. Dorenbos, J. Jansons, N. Khaidukov, Z. Rachko and J. Valbis. Experimental and theoretical studies of cross luminescence. Heavy Scintillators for Scientific and Industrial Applications, Editions Frontieres (Crystal 2000]), ISBN 2-86332-128-5, :161-166, 1993.
[29] W. Lehmann, Edge emission of n-type conducting ZnO and CdS. Solid-State Electronics, 9:1107-1110, 1966.
[30] J. S. Lapington and T. Conneely, Multi-channel picosecond photon timing with microchannel plate detectors, Nuclear Instruments & Methods in Physics Research Section a-Accelerators Spectrometers Detectors and Associated Equipment, 648:S186-189, 2010.
[31] J. Va'vra, PID techniques: Alternatives to RICH methods, Nuclear Instruments & Methods in Physics Research Section a-Accelerators Spectrometers Detectors and Associated Equipment, 639:193-201, 2011.
[32] D. Renker and E. Lorenz, Advances in solid state photon detectors, JINST, 4:P04004 (2009).
[33] R. Berger, D.D. Rathman, B.M. Tyrrell, E.J. Kohler, M.K. Rose, R.A. Murphy, T.S. Perry, H.F. Robey, F.A. Weber, D.M. Craig, A.M. Soares, S.P. Vernon, and R.K. Reich, "A 64 × 64-Pixel CMOS Test Chip for the Development of Large-Format Ultra-High-Speed Snapshot Imagers," in IEEE Journal of Solid-State Circuits, vol.43, no. 9, pp. 1940-1950 (2008).
[34] R.K. Reich, B. Kosicki, D.D. Rathman, M.K. Rose, R.A. Murphy, R. Berger, "Method and system for distribution of an exposure control signal for focal plane arrays," U.S. Patent.7501634, March 10, 2009.
[35] A.T. Teruya, S.P. Vernon, J.D. Moody, W.W. Hsing. C.G. Brown, M. Griffin, A.S. Mead, V. Tran, "Performance of a 512 × 512 Gated CMOS Imager with a 250 ps Exposure Time," Proc. SPIE Vol. 8505, 85050F, pp.1-9 (2012).
[36] Eric Oberla, Jean-Francois Genat, Herve Grabas, Henry Frisch, Kurtis Nishimura, Gary Varner, A 15 GSa/s, 1.5 GHz Bandwidth Waveform Digitizing ASIC, preprint submitted to Elsevier.